



Article citation info:

Qian W, Zeng X, Huang S, Yin X. Reliability analysis of multi-site damage with failure dependency of the turbine based on flow-thermal-solid coupling analysis and the Monte Carlo validated simulations *Eksploracja i Niezawodność – Maintenance and Reliability* 2023; 25(3) <http://doi.org/10.17531/ein/168771>

## Reliability analysis of multi-site damage with failure dependency of the turbine based on flow-thermal-solid coupling analysis and the Monte Carlo validated simulations

Indexed by:



Wenxue Qian<sup>a,c,\*</sup>, Xianhai Zeng<sup>a,c</sup>, Shuanghui Huang<sup>a,c</sup>, Xiaowei Yin<sup>b</sup>

<sup>a</sup> School of Mechanical Engineering and Automation, Northeastern University, Shenyang 110819, China

<sup>b</sup> School of Mechanical, Shenyang Institute of Engineering, Shenyang 110136, China

<sup>c</sup> Key Laboratory of Vibration and Control of Aero-Propulsion Systems, Ministry of Education, Northeastern University, Shenyang 110819, China

### Highlights

- The stress distribution of the turbine under multiple loads is determined by the flow-thermal-solid coupling analysis method.
- The stress distribution with dispersion characteristics is obtained through the coupling analysis process and response surface method.
- This reliability analysis model considers the failure dependency between the failure sites.
- The accuracy of this reliability model is verified by Monte Carlo simulation.

### Abstract

The harsh environmental loads may lead to strength failure in the turbine in an aero-engine. To accurately assess the strength reliability of the turbine under multiple loads, the stress distributions of 41 danger sites of a turbine under thermal, centrifugal, and pneumatic loads were determined by the flow-thermal-solid coupling analysis using ANSYS. Second, based on the flow-thermal-solid coupling analysis and response surface method, the probabilistic analysis model of stress at the danger site was established. And the probabilistic distribution of stress was determined by sampling and hypothesis testing. Finally, the reliability model of the turbine with multi-site damage and failure dependency was established, by which a reliability of 0.99802 was calculated. And the actual reliability of the turbine was 0.99626 determined by the Monte Carlo simulations, which verified the model in precision. The results indicated that the reliability model has a high efficiency and higher precision than the traditional reliability model with failure independence.

### Keywords

flow-thermal-solid coupling analysis, Monte Carlo simulation, turbine disk, multiple loads, probabilistic modeling, system reliability with failure dependency.

This is an open access article under the CC BY license (<https://creativecommons.org/licenses/by/4.0/>)

### 1. Introduction

Aero engines power the aircraft in flight and their reliability directly affects the safety of the aircraft. Current aircraft missions reflect greater diversity and specialization [24], which requires engines with lighter materials and greater performance [36]. The core of an aero engine is a highly complex structure that mainly contains a turbine, a combustion chamber, and a compressor. In recent years, numerous engine turbine rotors failed as a result of their broken and fractured rotor blades,

fatigue of the metal of the turbine disk, excessive deformation due to high temperatures, and many other reasons, while triggering a continuously increasing number of discussions and studies [17, 25, 26].

Strength-based failure of a turbine is mainly caused by excessive load or insufficient strength [42]. The multi-field environmental loads on turbine rotors deserve focused attention in turbine failure analysis, including centrifugal load,

(\*) Corresponding author.

E-mail addresses:

W. Qian (ORCID: 0000-0001-7271-8597) [wxqian@mail.neu.edu.cn](mailto:wxqian@mail.neu.edu.cn), X. Zeng [18879967890@qq.com](mailto:18879967890@qq.com), S. Huang [huangshuanghui0108@163.com](mailto:huangshuanghui0108@163.com), X. Yin [yinxw@sie.edu.cn](mailto:yinxw@sie.edu.cn)

aerodynamic load, and thermal load [19]. The performance of the turbine rotor significantly degrades in operation under high temperatures [16, 20, 39]. The large temperature gradient causes higher thermal stresses in vital sites [33]. And the high rotational speed leads to high centrifugal stresses in the turbine, which subsequently causes structural yielding [18]. Compared with other techniques such as the finite difference method (FDM) and method of moments (MOM), the fluid-thermal-solid coupling finite element analysis demonstrates greater efficiency and flexibility in structural analysis [5]. Therefore, it is extensively applied in industrial fields such as aviation, aerospace, marine, and nuclear engineering. Yazan discussed the influence of the heat pipe on the steady-state and transient temperature variations of the integral turbine in heat transfer analyses [35]. Balachandra applied the finite element method in the failure analysis of turbine blades and found friction as a reason for the failure of cantilever blades [3]. Yang performed a transient coupling analysis of the turbine rotor considering thermal load, centrifugal load, and preload jointly to determine the temperature distribution and stress distribution of the structure [21]. According to related research, most of the high-stress regions of turbine rotors under complex loading environments were distributed near the central holes of the turbine disks [10, 18], the mortise, and the blades [49]. In general, these high-stress regions are often the first sites to fail, i.e., the danger sites.

During operation, loading parameters such as pre-turbine temperature and speed are usually not constant but random variables [40]. And the production and assembly are also random processes to some extent. Therefore, the performances of the turbine are not constant, but obey a probability distribution [23]. Due to these uncertainties, the failure of the turbine shows significant dispersion in nature, namely exposing reliability problems [6]. According to research on turbines, probabilistic analysis methods are widely used to investigate the problems such as probabilistic low cycle fatigue life prediction of turbine disks and their reliability assessment [13, 34, 50], the probabilistic response of high-pressure turbine tip clearance [9], creep-fatigue failure of turbine disks [7, 37], and optimization of geometric parameters of turbine blades [14]. Probabilistic analysis is necessary for accurate failure prevention and reliability assessment of turbines [38]. Currently, probabilistic

analysis methods based on surrogate models, such as response surface methods (RSM) [27, 41], artificial neural networks (ANN) [1, 46], Kriging [11], and radial basis functions (RBF), are extensively promoted and applied in engineering. Fan proposed a surrogate model based on local maximum entropy (LME) theory in reliability analysis and sensitivity analysis of turbine disks with random geometric parameters [8]. These surrogate models demonstrated great efficiency and adaptability in reliability research on turbines compared to the traditional Monte Carlo method [2, 4, 28]. But the precisions of these methods were hard to guarantee, especially when the objects were complex structures or systems with multiple uncertainties and failure dependence.

For turbine structures, there are multiple sites in the structure that tend to damage due to the geometric complexity and loading diversity [31, 32]. In systems with variable amplitude loads, there will be a statistical dependency between the failure of each danger site [30]. This situation is similar to the failure of a system with multi-site damage. Due to randomness in production, manufacturing, and operation, the stress and deformation of the turbine rotor obey a probability distribution. Therefore, the site where the failure occurs first is variable [15, 22]. The stress-strength interference (SSI) model and its derivatives conveniently reflect the effects of random and common cause failure (CCF) on system failure [47, 51]. However, it is difficult for the SSI model to be applied directly to the reliability analysis of complex systems in most situations because of the uncertain distributions of load and strength. There are multiple danger sites on the turbine rotor. And the failure of any site will lead to the failure of the entire turbine rotor. In addition, the failures of danger sites are not simply independent due to the randomness of the loads but are dependent [29]. Traditional perspectives of independent failure consider the reliability of a system to be equal to the logical product of the reliability of the parts. For a mechanical structure, these views are not appropriate. and their evaluation of system reliability often deviates from the actual reliability. For systems with failure dependency, CCF is prevalent. And reliability analysis models with failure dependency are required. Xie et al developed a series of failure-dependent system reliability models through the minimum order statistics of strength based on the failure mechanism of the system [42-45]. On this basis,

Gao investigated in depth the multi-state dynamic fuzzy reliability problem using generating function and explored the effect of failure dependency on the reliability level of the system [12]. Zhao proposed an adapted reliability analysis model of improved dynamic failure-dependent systems for rotor blade systems such as aero-engine turbines with severe degradation and catastrophic failures [48]. Currently, failure-dependent system reliability models are attracting increasing attention.

In this paper, the reliability of a short-life engine turbine rotor for missiles was investigated: the flow-thermal-solid coupling analysis method was applied to study the characteristics of all danger sites of the turbine under thermal, centrifugal, and pneumatic loads; and the response surface method was applied to determine the dispersion of the load; then the mathematical analysis model of the reliability of turbine

strength failure was established with the failure dependency considered; finally, the Monte Carlo method was used to verify the feasibility of the model.

## 2. Flow-thermal-solid coupling analysis of turbine

### 2.1. Pre-processing of the turbine model

Fig. 1 shows an explosion view of a 3D model of a turbine engine for a missile. From left to right are the turbine shaft, bolts, turbine washer, turbine disk, and nuts. In this case, the left end of the shaft is connected to the compressor by key connections. And the right end face of the shaft is connected to the turbine by bolted connections. Among them, the turbine contains 41 integral blades mounted on the disk, which is the key component for the load bearing. However, the turbine disk is small, with a maximum diameter of only 140 mm.

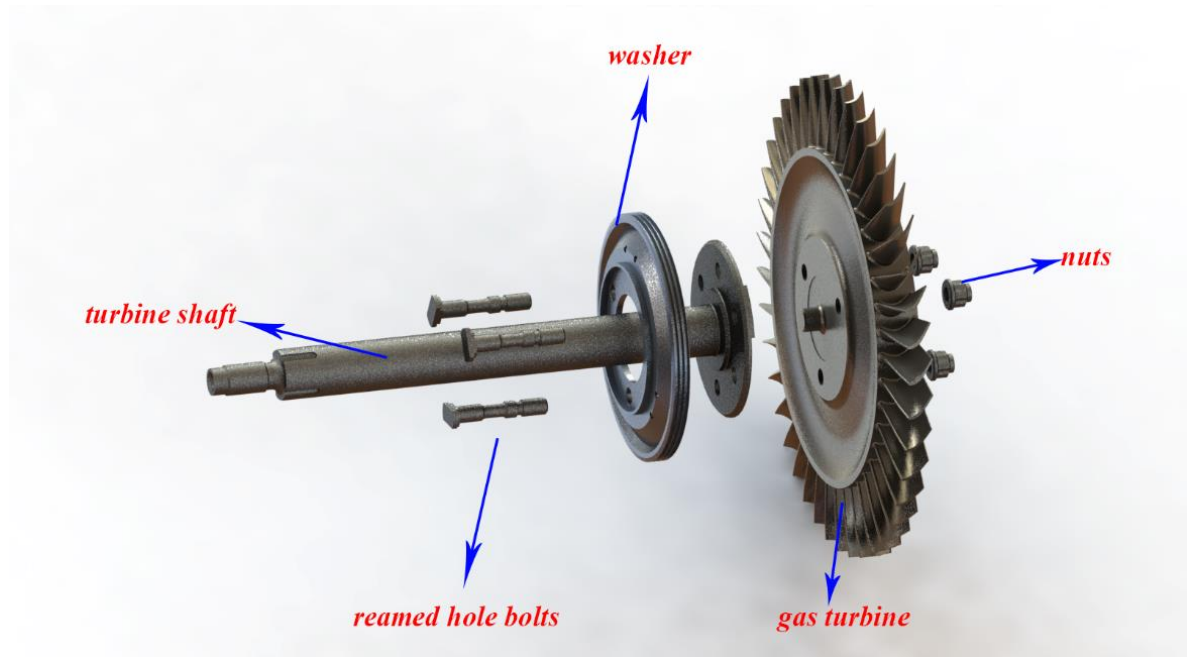


Figure 1. 3D explosion view of the turbine.

The turbine is mainly subjected to the thermal load, the centrifugal load, and the pneumatic load in operation. Among them, the centrifugal load mainly comes from the high-speed rotation of the turbine; the pneumatic load mainly results from the impact pressure caused by the high-speed mixed gas flow on the blades; and the large temperature gradient on the turbine is the main cause of thermal load.

Structurally, the original 3D model of this turbine, as shown in Fig. 2. a, does not possess periodic symmetry, which leads to the fact that the turbine cannot be simplified directly by sectors. However, it is most effective to simplify the original model to

improve the efficiency of the analysis. To facilitate the analysis of finite elements, the bolt holes, some rounded corners, and chamfers were removed, as shown in Fig. 2. b. Secondly, the model was dissected according to the sectors to build the single-blade model shown in Fig. 2. c. Tetrahedral elements and hexahedral elements were used to jointly divide the simplified model using the finite element analysis software ANSYS-19.0. Finally, the finite element model of the turbine was established by 62,057 nodes and 34,984 elements with high-quality grids, as shown in Fig. 2. d.

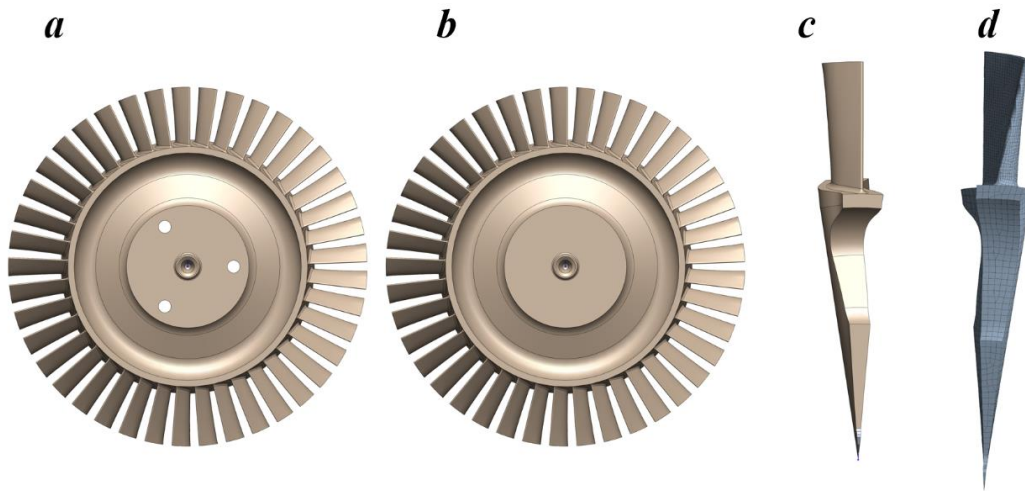


Figure 2. All 3D models in the pre-processing process. (a) The original model. (b) The simplified model. (c) The single-sector model. (d) The meshing model.

## 2.2. Fluid analysis

Fluid analysis is performed in ANSYS/CFX. A 3D model of the fluid domain was constructed based on the turbine model (Fig. 2. c) and meshed as shown in Fig. 3. a. The inflation was generated on the fluid surface in contact with the blade, which was a thin layer of flow considering the situation that the non-

negligible viscous force was immediately adjacent to the object surface in the high Reynolds number disturbance flow. Finally, fluid dynamics elements were used to divide the fluid domain. And the fluid domain of the turbine was established by 958,433 nodes and 34,984 elements with high-quality grids. The details are shown in Fig. 3. b, Fig. 3. c, and Fig. 3. d.

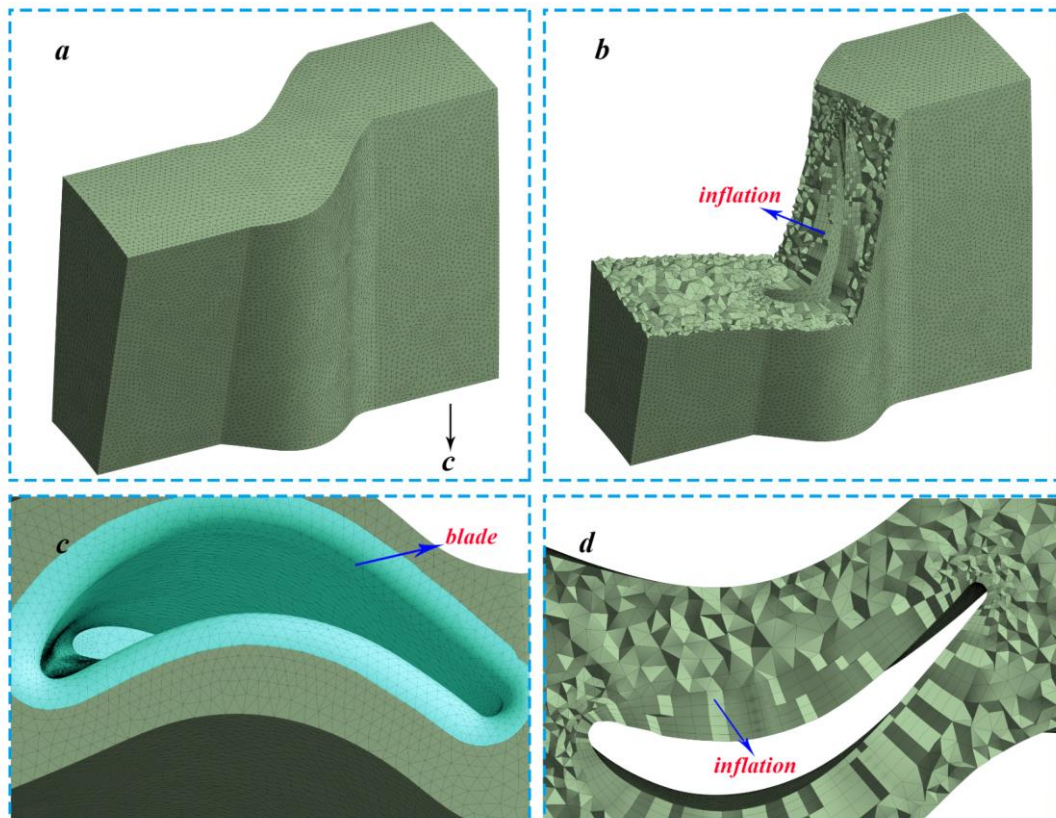


Figure 3. Details of the fluid mesh.

Table 1. Specific values for the parameters about multiple loads.

Parameters	The pre-turbine temperature, $T_a$ , K	The post-turbine temperature, $T_b$ , K	Gas flow rate, $Q$ , kg/s	Maximum speed value, $v$ , rpm	The outlet pressure, $P$ , Pa
Value	1,000	823	0.0224	50,000	190,000

According to the flow direction and the various load parameters listed in Tab. 1, the properties of the inlet, outlet, shroud, hub, and other boundary conditions were defined. The inlet was selected as the mass flow inlet, where the flow rate and inlet temperature (the pre-turbine temperature) were set to 0.0224 kg/s and 1000 K, respectively; the outlet was selected as the pressure outlet, where pressure was set to 1.9 Bar; and the periodic symmetry boundary and other boundaries were defined. Finally, the established fluid domain is shown in Fig. 4.

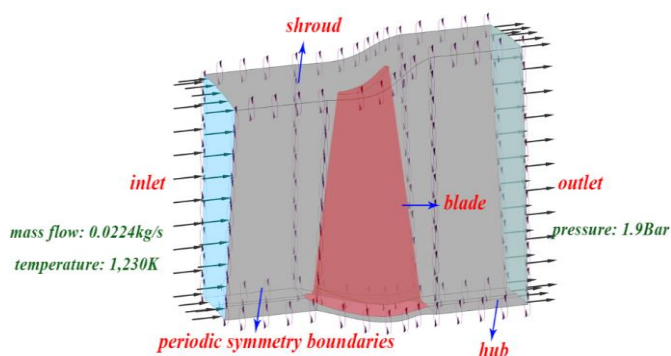


Figure 4. Boundaries of the fluid domain.

When the iterative calculation of the fluid domain was converged, the flow velocity, pressure distribution, and temperature distribution on the cross-section of the fluid domain and the blade surface were output, as shown in Fig. 5.

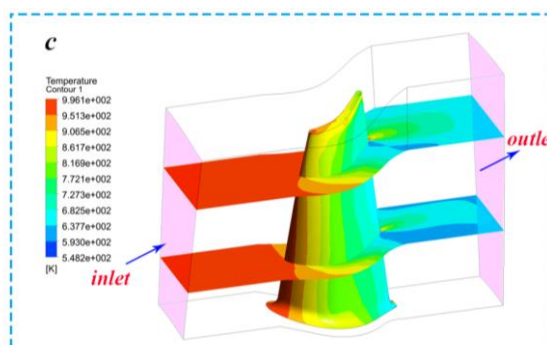
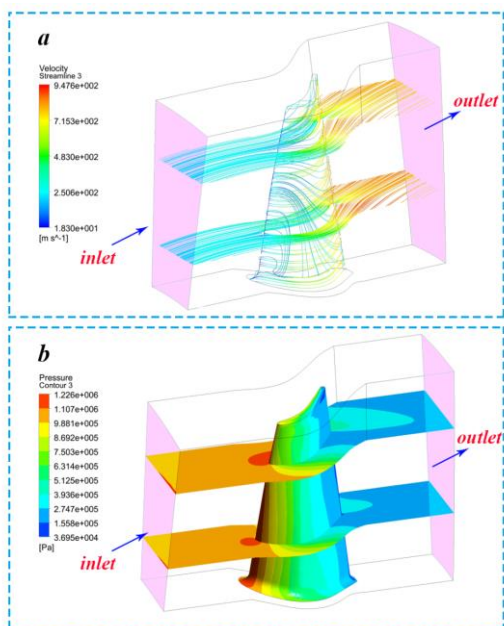


Figure 5. Post-processing of fluid analysis. (a) Fluid traces (b) pressure distribution (c) temperature distribution.

Among them, Fig. 5.a displays the flow traces in the fluid domain. And according to Fig. 5.b and Fig. 5.c, there is a large gradient of pressure and temperature near the surface of the blade, and the sites with the highest pressure and the highest temperature are both close to the surface of the blade.

### 2.3. Thermal analysis and structural analysis of turbine

The turbine is made of the nickel-based high-temperature alloy GH4169 (similar to Inconel 718 in the U.S. and NC19FeNb in France). This nickel-based alloy is widely used in critical structures such as rotor disks and blades of aero engines because of its excellent resistance to high temperature, oxidation, and corrosion. And Tab. 2 lists the values of the main parameters of GH4169 [20, 39].

Table 2. Values of the main parameters of GH4169.

Material	Density(kg/m <sup>3</sup> )	Elastic Modulus(MPa)	Poisson's Ratio	Coefficient of Thermal Expansion(K <sup>-1</sup> )	Yield Limit(MPa)	Strength Limit(MPa)
GH4169	8,240	203,000	0.3	11.8 × 10 <sup>-6</sup>	1,063	1,260

The results of the fluid analysis were imported into the thermal analysis module. Because the blade surface was in direct contact with hot gases, the temperature and pressure of the blade surface were extracted and defined as a boundary condition for the thermal analysis. The pre-turbine temperature and the post-turbine temperature were set at the end faces of the turbine, respectively. And the temperature distribution of the turbine was output after solving, as shown in Fig. 6.

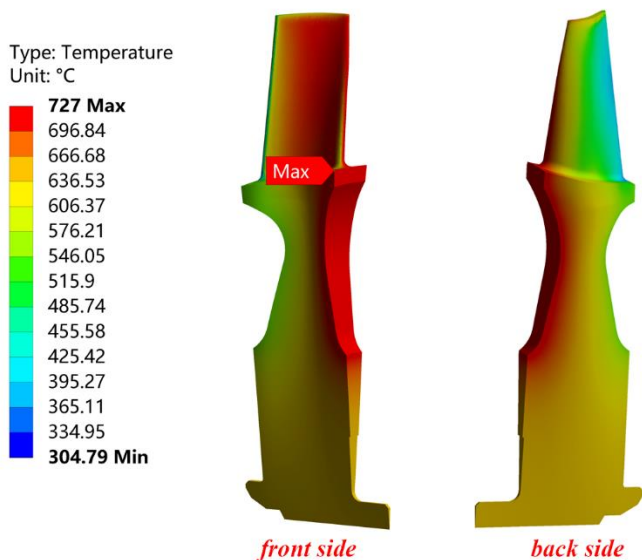


Figure 6. Temperature distribution diagram.

The distributions of temperature and pressure were imported into the static structural analysis module, which were considered as thermal and pneumatic loads, respectively. And the rotational speed of 50,000 rpm was applied to the disk. Then the axial displacement constraint and the circumferential displacement constraint were defined on the end face and the profile of the wheel, respectively.

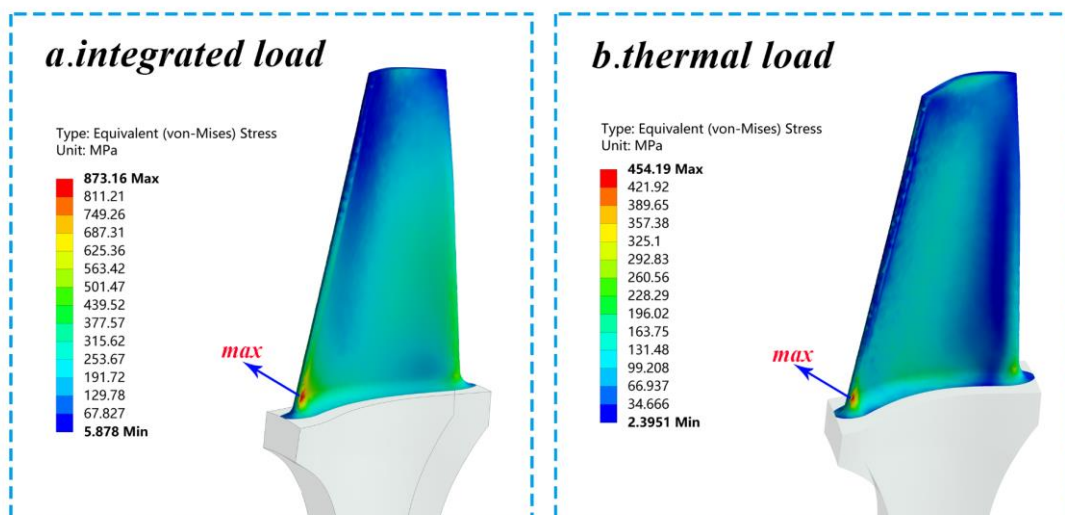
According to the results of the coupling analysis, the stress level of the turbine disk is lower, and all high stress sites are distributed in the blades. And the site with the maximum stress

of the turbine blade under multiple loads including centrifugal load, pneumatic load, and thermal load, superimposed appears at the root of the blade at the airflow inlet, with a maximum stress value of 873.16 MPa, as shown in Fig. 7. a.

Applying one of the loads to the original model alone, the stress distribution of the turbine blade under the centrifugal load, pneumatic load, and thermal load alone was all clear. When the centrifugal load was applied alone, the maximum stress site appeared in the blade basin near the inlet, with a maximum stress of 419.18 MPa, as shown in Fig. 7.b. When the pneumatic load was applied alone, the site with maximum stress appeared in the blade root at the outlet, with a maximum stress of 10.11 MPa, as shown in Fig. 7.c. When the thermal load was applied alone, the maximum stress site appeared at the root blade at the inlet, with a maximum stress of 454.19 MPa, as shown in Fig. 7.d. And the results of the finite element analysis of the turbine under different loading environments are summarized in Tab. 3. According to the coupling analysis, the thermal load and centrifugal load have a great influence on the stress distribution at the danger site, which are the critical loads of the turbine during operation; while the influence of the pneumatic load on the stress distribution at the danger site is negligible relatively.

Table 3. Summary of finite element analysis.

Material	Multiple loads	Thermal load	Centrifugal load	Pneumatic load
Danger site	At the root blade at the inlet	At the root blade at the inlet	At the blade basin near the inlet	At the blade root at the outlet
The maximum stress value (MPa)	873.16	454.19	419.18	10.113



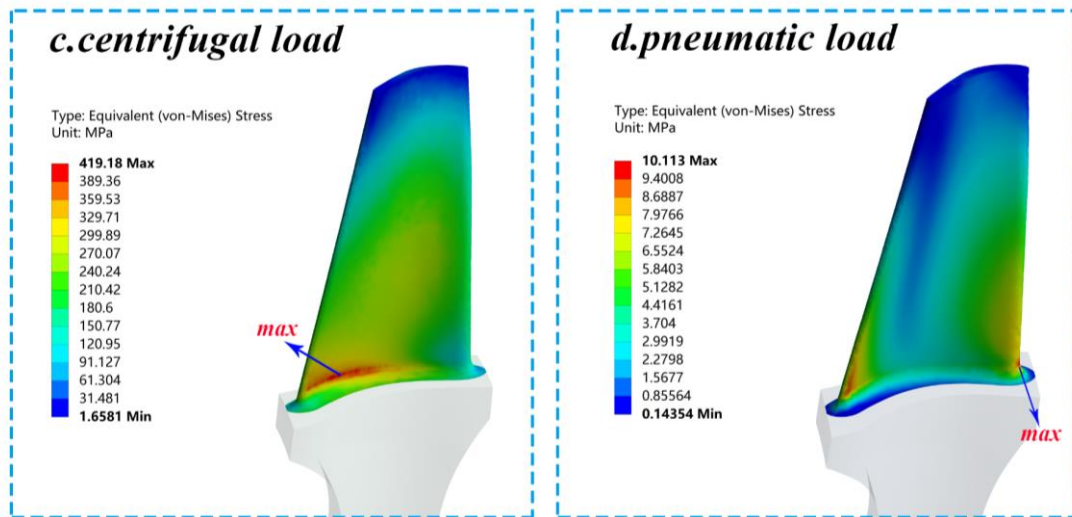


Figure 7. Turbine blade stress diagram.

### 3. Probabilistic analysis of stress at the danger sites

#### 3.1 Dispersion of parameters about loads and material

Due to the prevalent randomness in the manufacturing, assembly, and operation of the turbine, the load and material parameters are not constant but obey a probabilistic distribution. In the coupling analysis, the rotational speed, inlet temperature, material density, and the elastic modulus of the material were all set to specific values. However, it is not appropriate to neglect randomness in operation in reliability analysis for the turbine. Therefore, a probabilistic analysis of the turbine is necessary.

According to the coupling analysis, four key parameters including rotational speed, material density, turbine inlet temperature, and elastic modulus at room temperature were selected as factors affecting the stress at the danger site (at the blade root at the inlet). And appropriate coefficients of variation were formulated according to the operating parameters of the turbine and the published literature on the subject, as shown in Tab. 4.

Table 4. The distribution characteristics of four factors

Factors	Units	Distribution type	Mean value	Coefficient of variation
Maximum speed value, $v$	Rpm	Normal distribution	50,000	0.02
Material density, $\rho$	Kg/m <sup>3</sup>	Normal distribution	8,240	0.02
Inlet temperature, $T_a$	K	Normal distribution	1,000	0.05
Elastic modulus at room temperature, $E$	MPa	Normal distribution	203,000	0.02

#### 3.2 Response surface models of the stress at the turbine danger points

The response surface methodology is a statistical method for solving multivariate problems. First, a reasonable experimental design method is adopted and certain data are obtained through experiments; second, a multiple quadratic regression equation is used to fit the functional relationship between response and factors; finally, the regression equation is analyzed to find the optimal parameters in the process. Suppose that the variable  $Y$  is affected by  $n$  uncorrelated factors  $X(X_1, X_2, \dots, X_n) n \in Z$ , that is  $Y = f(X)$ . In practice, it is very difficult or impossible to find the true function between  $Y$  and  $X$  directly. However, the data points  $P(X, Y)$  can be obtained from the experiment according to certain principles. and the data are fitted into a response surface function by a quadratic polynomial, as shown in Eq. (1) [10].

$$Y = A + BX + XC^T X = g(X) \quad (1)$$

where  $A$ ,  $B$ , and  $C$  are the coefficient matrices of the response surface model.  $B$  and  $C$  are expressed as follows:

$$B = [b_1, b_2, b_3, \dots, b_n]$$

$$C = \begin{pmatrix} c_{11} & \dots & c_{1n} \\ \vdots & \ddots & \vdots \\ c_{n1} & \dots & c_{nn} \end{pmatrix}$$

With sufficient accuracy, the fitted response surface function can be used instead of the real model for the efficiency in subsequent analysis, that is  $f(X) \approx g(X)$ .

During the finite element analysis, the stress at the turbine danger site ( $S$ ) is affected by four independent critical factors

including rotational speed, material density, turbine inlet temperature, and elastic module at room temperature, that is  $\sigma = (\nu, \rho, T_a, E)$ .

Based on the distribution characteristics provided in Tab. 4, the simulated test programs were determined based on the Box-Table 5. Summary of simulations.

Behnken design (BBD) method in the response surface module, which contained 29 groups of simulations. Then all simulations were carried out according to the test programs, and the maximum stress values of the danger site at the root of the blade of each group were recorded, as shown in Tab. 5.

Run	Factor 1	Factor 2	Factor 3	Factor 4	Response
	Density, $\rho$ , kg/m <sup>3</sup>	Pre-turbine temperature, $T_a$ , K	Rotation speed, $\nu$ , rpm	Modulus of elasticity, $E$ , MPa	Stress at danger point, $\sigma$ , MPa
1	9,064	1000.00	50,000	182,700	882.82
2	8240	1000	45,000	182,700	807.76
3	9,064	900	50,000	203,000	824.83
4	7,416	1000	50,000	182,700	833.34
5	7,416	1000	50,000	223,300	856.76
6	9,064	1100	50,000	203,000	954.93
7	8,240	1000	50,000	203,000	873.28
8	8,240	1100	55,000	203,000	966.21
9	8,240	900	50,000	182,700	788.29
10	9,064	1000	50,000	223,300	908.21
11	8,240	900	50,000	223,300	812.63
12	8,240	1000	45,000	223,300	843.93
13	7,416	1100	50,000	203,000	927.89
14	8,240	1000	55,000	182,700	905.83
15	7,416	1000	55,000	203000	893.42
16	8,240	1100	50,000	223,300	952.22
17	8,240	1000	55,000	223,300	928.51
18	8,240	1000	50,000	203,000	873.28
19	7,416	1000	45,000	203,000	802.30
20	9,064	1000	55,000	203,000	938.91
21	8,240	1000	50,000	203,000	873.28
22	8,240	900	55,000	203,000	852.16
23	7,416	900	50,000	203,000	772.27
24	8,240	1100	45,000	203,000	912.05
25	8,240	1100	50,000	182,700	930.09
26	8,240	1000	50,000	203,000	873.28
27	9,064	1,000	45,000	203,000	846.87
28	8,240	1,000	50,000	203,000	873.28
29	8,240	900	45,000	203,000	747.85

Based on the test data in Tab. 5, a quadratic polynomial function was used to fit the response surface function of the stress at the danger site with respect to the four factors, as shown in Eq. (2). The meanings of the parameters in Eq. (4) are the same as those in Tab. 4.

$$\begin{aligned} \sigma = & -2745.51 + 0.152303 \times \rho + 2.28306 \times T_a \\ & + 0.0342948 \times \nu + 0.00229405 \times E \\ & - 7.74272 \times 10^{-5} \times \rho \times T_a \\ & - 1.85958 \times 10^{-5} \times T_a \times \nu \\ & - 3.32266 \times 10^{-8} \times \rho \times E \\ & - 2.88288 \times 10^{-6} \times \rho \times \rho \end{aligned} \quad (2)$$

The relationship between the response and the factors is approximated by the response surface model (Eq. (4)). By comparing the actual value of the response with the predicted value of the response surface model, it can be found that the response surface has high precision and can approximate the relationship between the response and the factors.

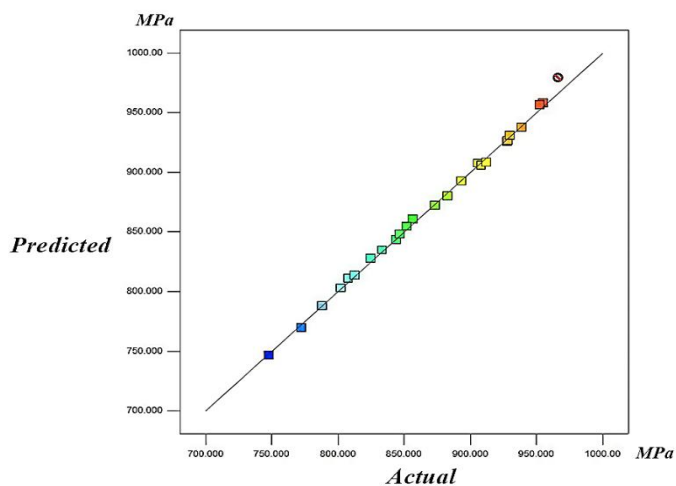


Figure 8. Predicted responses by response surface model vs. actual responses.

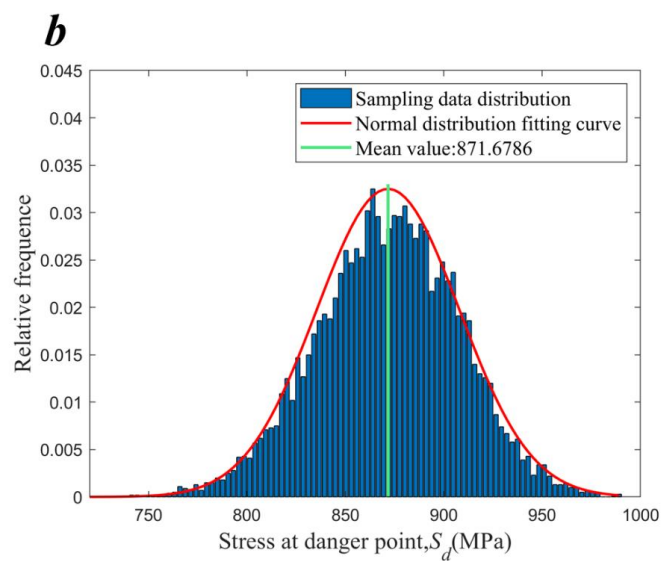
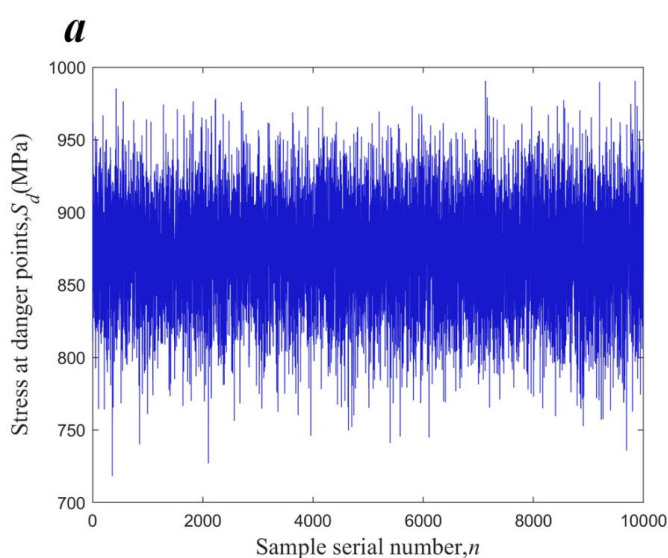


Figure 9. Probability distribution of stress at a danger site. (a) Sampling history. (b) Fitting.

### 3.3 Probability distribution of stress at danger sites

Based on Eq. (4), the four factors were sampled 10000 times according to their distributions, with the sampling history shown in Fig. 9.a. The 10000 samples were fitted to a probability distribution of the stress at the danger site. After the KS test, the stress at the danger site at the blade root obeyed a normal distribution, i.e.  $\sigma \sim N(871.6876, 26.602)$  MPa, as shown in Fig. 9.b. Since the simplified turbine model has a periodic symmetric structure, the stresses at danger sites at the blades' root can be considered to be independently and identically distributed.

### 3.4 Sensitivity analysis

Sensitivity analysis is an essential step in probabilistic modeling and reliability analysis. In probabilistic analysis, it identifies the factors that have a significant impact on the response, while being able to quantify the specific level of influence of all factors on the response. The partial derivatives of the factors of the response surface function are solved to know the rate of variation of the response with respect to the factors, which is

also the sensitivity of the response with respect to the factors [34].

According to the results of sensitivity analysis, the pre-turbine temperature is the most significant factor affecting the stress at the danger site, while the modulus of elasticity has the least effect on the stress at the danger site, as shown in Fig. 10. Therefore, the influence of pre-turbine temperature should be focused in the optimized design of the turbine.

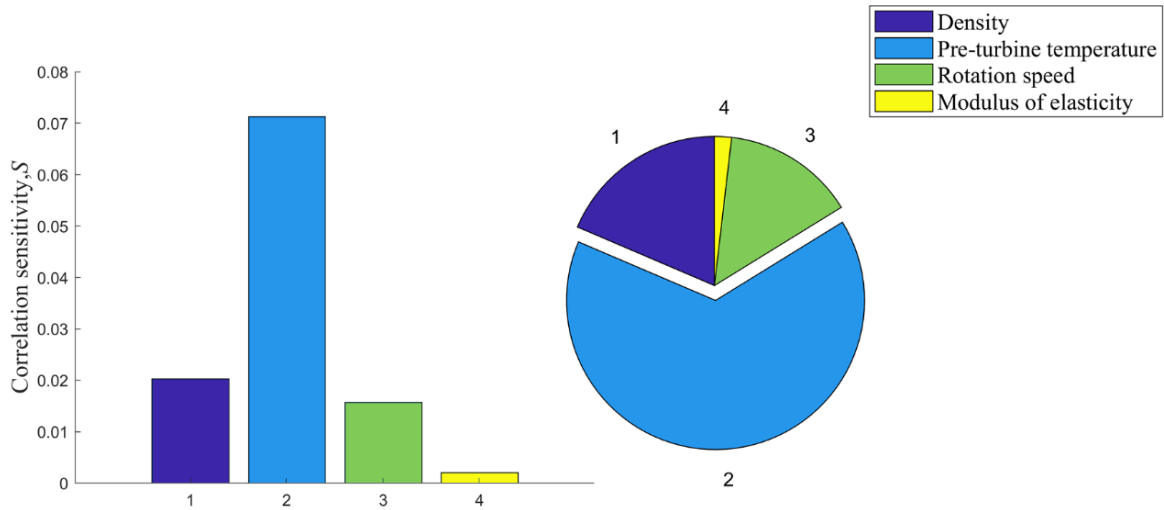


Figure 10 Sensitivity analysis results.

#### 4. The multi-site damage reliability model

There are 41 danger sites on this turbine that can be damaged, corresponding to each of the blades. And the failure of any one blade will lead to the failure of the whole turbine, which belongs to the series failure system. As there is a failure dependency among the blades, the turbine is a multi-site damage system with failure dependency. Failure of a mechanical structure is closely related to its strength and load. Theoretically, 'strength' and 'load' can be any pair of variables of the same magnitude but with a resistance relationship, such as stress, strain, temperature, etc.

This turbine belongs to a special class of aero-engine turbines with relatively short life and higher stress levels compared to others. In this case, the turbine is hardly subject to general fatigue failure. Therefore, it is generally considered that the turbine is safe once the stresses at the danger sites do not exceed their corresponding yield limits.

For any turbine danger site, when the strength is greater than the load, it is considered to be safe and reliable; conversely, it is dangerous. Stress is generally used to characterize the pair of interfering variables- strength and load. The load is the stress  $\sigma$  at that danger point, while the strength is the yield limit  $\sigma_s$  at that danger point. Then the failure state of the structure can be expressed by Eq. (3).

$$G = \sigma - \sigma_s \quad (3)$$

Where  $G \geq 0$  represents that the structure is failed, and  $G < 0$  represents that the structure is safe and reliable.

In fact, due to the prevalent randomness of the process from production to operation, the strength and load have a certain dispersion. Assuming that the strength and load of the structure obey certain distributions. Also,  $f(S)$  and  $h(s)$  denote the probability density function of strength and load, respectively, the reliability of the structure can be calculated by Eq. (4), which is also known as the load-strength interference (SSI) model [43].

$$R = \int_0^{+\infty} h(s) \left[ \int_s^{+\infty} f(S) dS \right] ds \quad (4)$$

Assume that the parts in a series system fail independently, the reliability of the system will be equal to the product of the reliability of the individual parts. Alternatively, if all parts in this system are the same in all aspects, then the reliability of the system can be calculated by Eq. (5).

$$R_s = \left\{ \int_0^{+\infty} h(s) \left[ \int_s^{+\infty} f(S) dS \right] ds \right\}^n \quad (5)$$

In a series system with failure dependency, there are multiple weak sites, all of which affect the failure of the system. System failure always starts with the weakest part, i.e., it is determined by the part of the system that fails first. Since the load and strength of each part are dispersed, the weakest part may be any part of the system. Assuming that the loads on all parts in a series system obey the same distribution, the reliability of the system is determined by the minimum statistic of the strength of the parts and the loads, as shown in Eq. (6) [42-45].

$$R_s = \int_0^{+\infty} h(s) \left[ \int_s^{+\infty} g_1(S) dS \right] ds \quad (6)$$

Where  $g_1(s)$  represents the probability density function of the minimum order statistic of parts' strength, and  $g_1(s)$  can be expressed by Eq. (7) [43].

$$g_1(S) = n[1 - F(S)]^{n-1}f(S) \quad (7)$$

After derivations, the system reliability can be expressed as Eq. (8) [43].

$$\begin{aligned} R_s &= \int_0^{+\infty} h(s) \left[ \int_s^{+\infty} n[1 - F(S)]^{n-1} f(S) dS \right] ds \\ &= \int_0^{+\infty} h(s) \left[ \int_s^{+\infty} \frac{-d[1 - F(S)]^n}{dS} f(S) dS \right] ds \\ &= \int_0^{+\infty} h(s) [1 - F(s)]^n ds = \int_0^{+\infty} h(s) \left[ \int_s^{+\infty} f(S) dS \right]^n ds \end{aligned} \quad (8)$$

According to the material datasheets, the yield limit  $\sigma_s$  of the nickel-based alloy GH4169 at 600°C approximately obeys a normal distribution with a mean value and standard deviation of 1003 MPa and 22 MPa, respectively. And the reliability analysis models of multi-site damage with failure dependency of the turbine were established based on Eq. (10), as shown in Eq. (9) and Eq. (10).

$$R_s = \int_0^{+\infty} h_a(s) \left[ \int_s^{+\infty} f_a(S) dS \right]^{41} ds \quad (9)$$

$$P_f = \int_0^{+\infty} h_a(s) \left[ \int_0^s f_a(S) dS \right]^{41} ds \quad (10)$$

where  $R_s$  and  $P_f$  denote the reliability and failure probability of the turbine, respectively. Also,  $f_a(s)$  and  $h_a(s)$  denote the probability density functions of the strength and load of the danger sites of the turbine, respectively.

And the reliability and failure probability of the turbine was calculated to be 0.99802 and 0.00198 by the model with failure dependency, respectively.

To verify the effects of the failure dependency on the reliability of the turbine disk system, a failure-independent reliability analysis model of the turbine disk is developed to verify it as Eq. (11) and Eq. (12):

$$R'_s = R_1^{41} = \left[ \int_0^{+\infty} h_a(s) \int_s^{+\infty} f_a(S) dS ds \right]^{41} \quad (11)$$

$$P'_f = 1 - R'_s \quad (12)$$

where  $R'_s$  and  $P'_f$  denotes the reliability and failure probability of the failure-independent system;  $R_1$  denotes the

reliability of only a failure site of the turbine;

And the reliability and failure probability of the turbine was calculated to be 0.92197 and 0.07803 by the model with failure independence, respectively.

## 5. Validation of the reliability model through the Monte Carlo simulation

The Monte Carlo simulation is a method based on simulated tests in which the failure process of a structure with dispersed loads and strengths is simulated through sampling. This method is highly operational and simple in principle, but relatively inefficient [2].

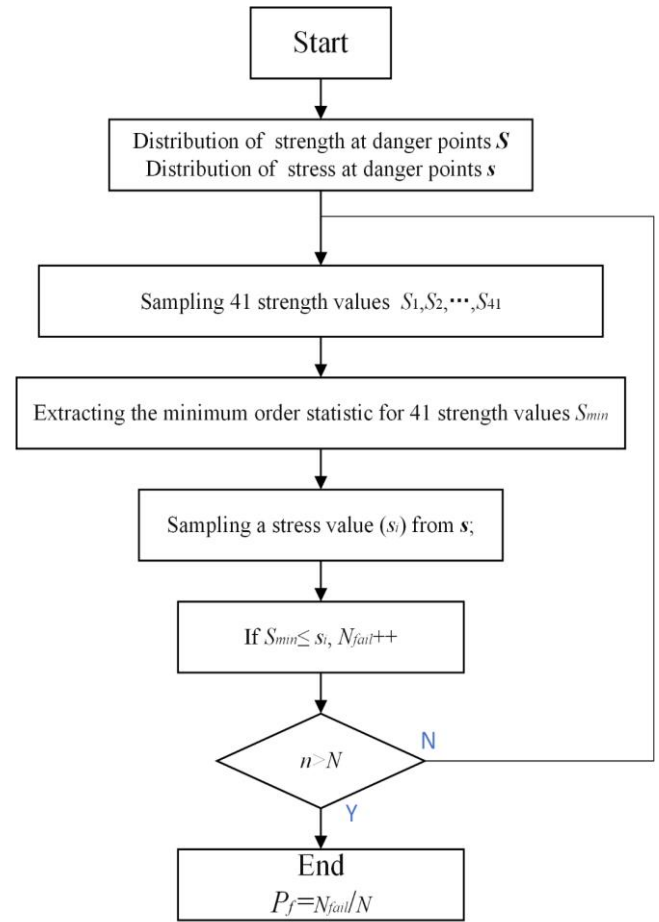


Figure 11. The framework of the Monte Carlo simulation.

The general processes of the Monte Carlo simulation are as follows: for the turbine, failure at any site can result in system failure. And the failure at the danger site is defined as its stress exceeding its yield strength. Since the simplified model has periodic symmetry, it can be assumed that danger sites have the same loads. Therefore, only one stress value is extracted from the load distribution in one simulation. The strength distribution of each danger site is the same but independent, so strength

values are extracted from the strength distribution of each danger site. Next, the minimum order statistics of the strength samples are retrieved and compared with the stress samples. The turbine is safe and reliable only when the minimum order strength statistics at all danger sites exceed their stresses. Otherwise, it becomes failed. At this point, one simulation is complete. With more simulations, the closer the overall sample distribution will be to the probability distribution of the actual turbine failure. Therefore, when the number of simulations is large enough, the ratio of the number of failures to the total number of simulations can be considered as the real probability of failure of the turbine. And the framework of the Monte Carlo simulation is shown in Fig. 11[4, 28].

According to the results of Monte Carlo simulations, a total of 50,000 tests were simulated returning 313 samples that a turbine fails. The probability of failure of the turbine was calculated to be 0.00626, while its reliability is 0.99374. These could be regarded as the real probability of failure and reliability of the turbine to verify the precision of the model with independent failure and the model with multi-site damage. And the results are recorded in the Tab. 6.

Table 6. Validation of three models in precision.

Model	Reliability	Probability of failure	The relative error in reliability /%
The Monte Carlo model	0.99374	0.00626	-
The model with failure dependency	0.99802	0.00198	0.4307
The model with failure independence	0.92197	0.07803	7.222

According to Tab. 6, the results of the model with failure dependency have a very high precision in reliability prediction with a relative error of just 0.4307% with real reliability. However, the results of the model with independent failures produce unacceptable errors from reality. It can be concluded that the reliability model with failure dependency is feasible in the prediction of reliability of complex system structures. The results also highlight the fact that the failure dependency among parts cannot be neglected in reliability investigations of complex mechanical structures like turbines.

## 6. Conclusions

To describe the possible failure situations of a turbine in operation, the reliability of a turbine under a complex environment with random loading was explored comprehensively with the applications of methods or ideas such as flow-thermal-solid coupling analysis, response surface method, multi-site damage correlation system, and Monte Carlo simulation. And the details of the conclusion are as follows:

1. The stress level at the danger site of a turbine under multiple loads, such as thermal, centrifugal, and aerodynamic loads, was determined by the flow-thermal-solid coupling analysis. And the location of the danger site appears at the blade root at the inlet with a maximum equivalent stress of 873.16 MPa.
2. Based on the dispersion of the factors in terms of material and loads, the response surface model of the stress at the danger site was established. with respect to these factors Then the probability distributions of the stresses at the danger sites were also determined, that is  $\sigma \sim N(871.6876, 26.602)$  MPa. Through sensitivity analysis, it was found that the pre-turbine temperature was the most influential factor on the stress at the danger point
3. The multi-site reliability analysis model with a turbine failure dependency was established and the turbine reliability was calculated as 0.99802.
4. The actual reliability of the turbine was 0.99626 obtained by Monte Carlo simulation, which examined the prediction precision of the model with failure dependency and the model with independence. The predictions of the model with failure dependency established in this paper were found to be quite close to the reliability calculated by Monte Carlo simulation, which emphasize the importance of failure dependency in reliability investigations of complex mechanical structures such turbines.

In this work, the proposed analysis strategy provides a technical guiding direction for the reliability assessment of turbine rotors. Moreover, it contributes to improve the reliability and maintenance cost-effectiveness of military and aerospace systems.

## Acknowledgments

This work was partially supported by the National Natural Science Foundation of China (Grant No. 52175131), the National Science and Technology Major Project of the Ministry of Science and Technology of China (Grant No. J2019-IV-0016-0084).

## References

1. Al-Garni A, Abdelrahman W, Abdallah A. ANN-based failure modeling of classes of aircraft engine components using radial basis functions. *Eksploatacja i Niezawodność – Maintenance and Reliability* 2019; 21(2): 311–317. <http://dx.doi.org/10.17531/ein.2019.2.16>.
2. Amirkhani S, Chaibakhsh A, Ghaffari A. Nonlinear robust fault diagnosis of power plant gas turbine using Monte Carlo-based adaptive threshold approach. *ISA transactions* 2020; 100: 171-184. <https://doi.org/10.1016/j.isatra.2019.11.035>.
3. Balachandra S P, Mishra R K, Prithvi S S, et al. Finite Element Approach for Failure Analysis of a Gas Turbine Blade. *Journal of Failure Analysis and Prevention* 2018; 18: 1210-1215. <https://doi.org/10.1007/s11668-018-0514-5>.
4. Behbahaninia A, Banifateme M, Azmayesh M H, et al. Markov and monte carlo simulation of waste-to-energy power plants considering variable fuel analysis and failure rates. *Journal of Energy Resources Technology* 2022; 144(6): 062101. <https://doi.org/10.1115/1.4051760>.
5. Dhamodaran M, Jegadeesan S, Praveen K R. Computation of the fluid flow and the temperature field by finite element modeling. *Cluster Computing* 2019; 22: 14505-14511. <https://doi.org/10.1007/s10586-018-2330-9>.
6. Dong X W, Li W K, Zhu C Y, et al. Dynamic reliability design of multicomponent structure with improved weighted regression distributed collaborative surrogate model method. *Advances in Materials Science and Engineering* 2018; 2018: 3832783. <https://doi.org/10.1155/2018/3832783>.
7. Esakki M S, Prakash R V, Mishra R K, et al. Thermo-mechanical fatigue life assessment of a gas turbine rotor through reliability approach. *Journal of Failure Analysis and Prevention* 2018; 18: 1361-1368. <https://doi.org/10.1007/s11668-018-0531-4>.
8. Fan J, Liao H, Wang H, et al. Local maximum-entropy based surrogate model and its application to structural reliability analysis. *Structural and Multidisciplinary Optimization* 2018; 57: 373-392. <https://doi.org/10.1007/s00158-017-1760-y>.
9. Fei C W, Choy Y S, Hu D Y, et al. Dynamic probabilistic design approach of high-pressure turbine blade-tip radial running clearance. *Nonlinear Dynamics* 2016; 86: 205-223. <https://doi.org/10.1007/s11071-016-2883-1>.
10. Gao H F, Bai G C, Gao Y, et al. Reliability analysis for aero-engine turbine disc fatigue life with multiple random variables based on distributed collaborative response surface method. *Journal of Central South University* 2015; 22(12): 4693-4701, <http://dx.doi.org/10.1007/s11771-015-3020-x>.
11. Gao H F, Wang A, Zio E, et al. Fatigue strength reliability assessment of turbo-fan blades by Kriging-based distributed collaborative response surface method. *Eksploatacja i Niezawodność – Maintenance and Reliability* 2019; 21(3): 530–538, <http://dx.doi.org/10.17531/ein.2019.3.20>.
12. Gao P, Xie L, Hu W, et al. Dynamic fuzzy reliability analysis of multistate systems based on universal generating function. *Mathematical Problems in Engineering* 2018; 2018: 1-8, <https://doi.org/10.1155/2018/6524629>.
13. Guan X, He J, Rasselkorde E M, et al. Probabilistic fatigue life prediction and structural reliability evaluation of turbine rotors integrating an automated ultrasonic inspection system. *Journal of Nondestructive Evaluation*; 2014, 33: 51-61. <https://doi.org/10.1007/s10921-013-0202-z>.
14. Heinze K, Meyer M, Scharfenstein J, et al. A parametric model for probabilistic analysis of turbine blades considering real geometric effects. *CEAS Aeronautical Journal*; 2014, 5: 41-51. <https://doi.org/10.1007/s13272-013-0088-6>.
15. Hossain M A, Cottingham J R, Stewart C M. An Extrema Approach to Probabilistic Creep Modeling in Finite Element Analysis. *Journal of Engineering for Gas Turbines and Power* 2022; 144(1): 1-10, <https://doi.org/10.1115/1.4052260>.
16. Khalesi J, Modaresahmadi S, Atefi G. SEM Gamma prime observation in a thermal and stress analysis of a first-stage Rene’80H gas turbine blade: numerical and experimental investigation. *Iranian Journal of Science and Technology, Transactions of Mechanical Engineering* 2019; 43: 613-626. <https://doi.org/10.1007/s40997-018-0235-0>.
17. Kolagar A M, Tabrizi N, Cheraghzadeh M, et al. Failure analysis of gas turbine first stage blade made of nickel-based superalloy. *Case Studies in Engineering Failure Analysis* 2017; 8: 61-68, <https://doi.org/10.1016/j.csefa.2017.04.002>.
18. Kumar R, Ranjan V, Kumar B, et al. Finite element modelling and analysis of the burst margin of a gas turbine disc using an area weighted

- mean hoop stress method. *Engineering Failure Analysis* 2018; 90: 425-433. <https://doi.org/10.1016/j.engfailanal.2017.12.014>.
19. Li L, Wan H, Gao W, et al. Reliability based multidisciplinary design optimization of cooling turbine blade considering uncertainty data statistics. *Structural and multidisciplinary optimization* 2019; 59(2): 659-673. <https://doi.org/10.1007/s00158-018-2081-5>.
  20. Liu L L, Hu D Y, Li D, et al. Effect of Grain Size on Low Cycle Fatigue Life in Compressor Disc Superalloy GH4169 at 600 °C. *Procedia Structural Integrity* 2017; 7: 174-181, <https://doi.org/10.1016/j.prostr.2017.11.075>.
  21. Liu Y, Yuan Q, Zhu G, et al. Transient analysis and design improvement of a gas turbine rotor based on thermal-mechanical method. *Shock and Vibration* 2018; 2018: 102950. <https://doi.org/10.1155/2018/1029520>.
  22. Lu C, Fei C W, Feng Y W, et al. Probabilistic analyses of structural dynamic response with modified Kriging-based moving extremum framework. *Engineering Failure Analysis* 2021; 125: 105398, <https://doi.org/10.1016/j.engfailanal.2021.105398>.
  23. Lu C, Feng Y W, Fei C W, et al. Probabilistic analysis method of turbine blisk with multi-failure modes by two-way fluid-thermal-solid coupling. *Proceedings of the Institution of Mechanical Engineers, Part C: Journal of Mechanical Engineering Science*, 2018, 232(16): 2873-2886, <https://doi.org/10.1177/0954406217723673>.
  24. Ma X B, Wang Z H, Guan T Y, et al. Aircraft reliability assessment for an individual mission based on recordable flight parameters. *Quality and Reliability Engineering International* 2018; 34(8): 1605-1614, <https://doi.org/10.1002/qre.2345>.
  25. Mishra R K, Thomas J, Srinivasan K, et al. Failure analysis of an un-cooled turbine blade in an aero gas turbine engine. *Engineering Failure Analysis* 2017; 79: 836-844, <https://doi.org/10.1016/j.engfailanal.2017.05.042>.
  26. Mojtaba R, Abbas B, Mohammad M, et al. Corrosion-Fatigue Failure of Gas-Turbine Blades in an Oil and Gas Production Plant. *Materials* 2020; 13(4): 900-907, <https://doi.org/10.3390/ma13040900>.
  27. Nowak G, Rusin A. Shape and operation optimisation of a supercritical steam turbine rotor. *Energy conversion and management* 2013; 74: 417-425. <https://doi.org/10.1016/j.enconman.2013.06.037>.
  28. Polat Ö, Eyüboğlu O H, Gül Ö. Monte Carlo simulation of electric vehicle loads respect to return home from work and impacts to the low voltage side of distribution network. *Electrical Engineering* 2021; 103(1): 439-445, <https://doi.org/10.1007/s00202-020-01093-5>.
  29. Qian W, Yin X, Xie L. Reliability modeling and assessment of component with multiple weak sites under complex loading. *Mathematical Problems in Engineering* 2014; 2014: 1-9, <https://doi.org/10.1155/2014/583803>.
  30. Ren J G, Zhao B F, Xie L Y, et al. Fatigue Reliability Analysis of a Compressor Disk Based on Probability Cumulative Damage Criterion. *Materials* 2020; 13(9): 1-15, <https://doi.org/10.3390/ma13092182>.
  31. Ruiz-Muñoz G A. Method to analyse multiple site damage fatigue before and after crack coalescence. *Engineering Fracture Mechanics* 2018; 188: 416-430, <https://doi.org/10.1016/j.engfracmech.2017.09.011>.
  32. Sakaris C S, Sakellariou J S, Fassois S D. Multi-site damage precise localization via the random vibration functional model based method: Formulation & concept validation. *Mechanical Systems and Signal Processing* 2021; 160: 107880, <https://doi.org/10.1016/j.ymsp.2021.107880>.
  33. Sawiński D, Ziókowski P, Badur J. Thermal failure of a second rotor stage in heavy duty gas turbine. *Engineering Failure Analysis* 2020; 115: 104672, <https://doi.org/10.1016/j.engfailanal.2020.104672>.
  34. Song L K, Bai G C, Fei C W. Probabilistic LCF life assessment for turbine discs with DC strategy-based wavelet neural network regression. *International Journal of Fatigue* 2019; 119: 204-219. <https://doi.org/10.1016/j.ijfatigue.2018.10.005>.
  35. Taamneh Y. Thermal analysis of gas turbine disk integrated with rotating heat pipes. *Case studies in thermal engineering* 2017; 10: 335-342. <https://doi.org/10.1016/j.csite.2017.09.002>.
  36. Tiassou K, Kanoun K, Kaàniche M, et al. Aircraft operational reliability—A model-based approach and a case study. *Reliability Engineering & System Safety* 2013; 120: 163-176, <https://doi.org/10.1016/J.RESS.2013.07.008>.
  37. Tomevenya K M, Liu S J. Probabilistic fatigue-creep life reliability assessment of aircraft turbine disk. *Journal of Mechanical Science and Technology* 2018; 32: 5127-5132. <https://doi.org/10.1007/s12206-018-1010-2>.
  38. Vahid-Pakdel M J, Mohammadi-Ivatloo B. Probabilistic assessment of wind turbine impact on distribution networks using linearized power flow formulation. *Electric Power Systems Research* 2018; 162: 109-117. <https://doi.org/10.1016/j.epr.2018.05.001>.
  39. Wang R Z, Zhang X C, Gong J G, et al. Creep-fatigue life prediction and interaction diagram in nickel-based GH4169 superalloy at 650 C based on cycle-by-cycle concept. *International Journal of Fatigue* 2017; 97: 114-123. <https://doi.org/10.1016/j.ijfatigue.2016.11.021>.

40. Wang R, Liu X, Hu D, et al. Zone-based reliability analysis on fatigue life of GH720Li turbine disk concerning uncertainty quantification. *Aerospace Science and Technology* 2017; 70: 300-309. <https://doi.org/10.1016/j.ast.2017.08.011>.
41. Wei Y, Bai G, Wang B, et al. Reliability Analysis on structures based on a modified iterative response surface method. *Mathematical Problems in Engineering* 2018; 2018: 1-14, <https://doi.org/10.1155/2018/8794160>.
42. Xie L Y, Wang Z, Lin W Q. System fatigue reliability modeling under stochastic cyclic load. *Int. J. of Reliability and Safety* 2008; 2(4): 357-367, <https://doi.org/10.1504/IJRS.2008.022081>.
43. Xie L Y, Zhou J Y, Hao C Z. System-level load-strength interference based reliability modeling of k-out-of-n system. *Rel. Eng. & Sys. Safety* 2003; 84 (3): 311-317, <https://doi.org/10.1016/j.res.2003.12.003>.
44. Xie L, Wu N, Qian W. Time domain series system definition and gear set reliability modeling. *Reliability Engineering & System Safety* 2016; 155: 97-104, <https://doi.org/10.1016/j.res.2016.06.009>.
45. Xie LY, Zhou J Y, Wang Y Y, et al. Load- Strength Order Statistics Interference Models for System Reliability Evaluation. *International Journal of Performability Engineering* 2005; 1(1): 23-36,
46. Zhang C Y, Wei J S, Wang Z, et al. Creep-Based Reliability Evaluation of Turbine Blade-Tip Clearance with Novel Neural Network Regression. *Materials* 2019; 12(21): 3552-3573, <https://doi.org/10.3390/ma12213552>.
47. Zhang S, Lv R N, Si S B, et al. Reliability Analysis of Systems with Common Cause Failure Based on Stress-Strength Interference Model. *Journal of Shanghai Jiaotong University (Science)* 2018; 23(5): 707-710, <http://doi.org/10.1007/s12204-018-1968-z>.
48. Zhao B F, Xie L Y, Zhang Y, et al. An improved dynamic load-strength interference model for the reliability analysis of aero-engine rotor blade system. *Proceedings of the Institution of Mechanical Engineers, Journal of Aerospace Engineering* 2021; 235(11): 1355-1373, <https://doi.org/10.1177/0954410020972898>.
49. Zhao Y J, Chen L, Li H, et al. Structural dynamic reliability estimation with advanced extremum Kriging method. *IOP Conference Series Materials Science and Engineering* 2021; 1043(5): 052030, <https://doi.org/10.1088/1757-899X/1043/5/052030>.
50. Zhu S P, Huang H Z, Smith R, et al. Bayesian framework for probabilistic low cycle fatigue life prediction and uncertainty modeling of aircraft turbine disk alloys. *Probabilistic Engineering Mechanics* 2013; 34: 114-122. <https://doi.org/10.1016/j.probenmech.2013.08.004>.
51. Zhu S P, Liu Q, Zhou J, et al. Fatigue reliability assessment of turbine discs under multi-source uncertainties. *Fatigue & Fracture of Engineering Materials & Structures* 2018; 41(6): 1291-1305, <https://doi.org/10.1111/ffe.12772>.